Hard Elastic Behavior in Polyurethane Foams

C. KAU,[1] L. HUBER,[2] A. HILTNER,[1] and E. BAER[1,*]

[1]Department of Macromolecular Science, Case Western Reserve University, Cleveland, Ohio 44106;
[2]The Dow Chemical Company, Freeport, Texas 77540

SYNOPSIS

Hard elastic behavior is characterized by high porosity and high recoverability from large strain, and initial Hookean elasticity was discovered in polyurethane foams containing styrene–acrylonitrile (SAN) copolymer particles. The presence of SAN particles introduces a heterogeneous morphology, and when the foam was strained in the SEM, it was observed that the struts became highly porous with profuse voiding nucleated by the SAN particles. It was found that these flexible polyurethane foams had a similar morphological structure in the strained struts as did the typical hard elastic materials. The phenomenon of stress depression, when foam specimens under stress were subjected to nonswelling liquids, was utilized to probe the role of surface stress in these hard elastic foams. An analytic methodology established for other highly porous hard elastic materials based on stress depression was utilized to obtain the average distance between voids in the struts. The calculated values were in good agreement with direct scanning electron microscopy observations, confirming that voiding initiated at the boundaries of SAN particles.

INTRODUCTION

Both the load-bearing capacity and dynamic fatigue performance of flexible polyurethane (PU) foams, which are affected by irreversible deformation processes, have become important issues in deciding foam applicability. It is well known that the compressive stress–strain behavior of flexible PU foam can be qualitatively described initially by a linear elastic behavior, which is then followed by a plateau region in the curve and, subsequently, by a densification region. An understanding of this deformation behavior has been previously associated with the bending, buckling, and compaction of cell struts. When a flexible PU foam is subjected to cyclic compressive deformation, it is found the initial modulus and the load-bearing capacity at maximum compression decrease with an increasing number of loading cycles.[1-3] Most previous investigators hypothesized that the reduction of load-bearing capacity is due to molecular effects such as the rearrangement of the hydrogen bonding between the macromolecule chains of the urethane material and tried to confirm this hypothesis by changing the ingredients in the foam formulation and the isocyanate index.[4-7] Turner and Wilkes[8] studied the morphology of flexible PU foams and observed that higher water content in the formulation resulted in a greater population of discontinuous urea precipitates with a particle size of around 3000 Å that increase the modulus. Although many attempts to improve the irreversible deformation resistance in PU foams have been made through chemical modification, direct observation describing the onset of irreversible deformation in the cell struts of the foam have not been as widely investigated.

Based on the results of our previous study,[3] a microcrack or a crazelike structure appears on the tension side of the flexed cell strut when the foam is subjected to large compressive deformation. Lee[9] reported related results at very low magnification after both dynamic and static fatigue loading. During compressive cyclic loading, flexible PU foam emits profuse acoustic emission signals.[3] The composition with the highest content of styrene–acrylonitrile copolymer (SAN) in the form of spherically shaped particles of around 2000–3000 Å gave enormous acoustic emission in the early cycles of the loading

* To whom correspondence should be addressed.

Journal of Applied Polymer Science, Vol. 44, 2081–2093 (1992)
 CCC 0021-8995/92/122081-13$04.00

history. Corresponding trends of decreasing load-bearing capacity at the maximum compression of each loading cycle was observed. It is believed that the presence of SAN particles in flexible PU foams introduces a heterogeneous morphology that creates sites for localized stress concentration. Although these SAN particles increase the modulus as well as the plateau stress, these particles cause the onset of crazing during large deformation in compression. The observed damage evolution indicates that the irreversible deformation in cell struts is caused by profuse crazing and microcracking, which explains both the large acoustic emission and the deterioration of the load-bearing capacity of the foam.

Craze formation in solid PU elastomers at high elongation (>500% strain) was previously observed[10] and attributed to the development of crazes that emanate from heterogeneities arising from strain-induced crystallinity occurring in PU elastomers. Crazes in elastomeric PUs also occur during biodegradation,[11] and, again, it is suggested that the crazing phenomenon is due to a heterogeneous structure within the PU. Subsequently, it is not surprising that crazing could occur in the strut of a flexible PU foam containing small hard SAN particles.

The profuse crazing phenomenon is commonly observed in a variety of crystalline and amorphous polymers, and the only requirement to develop this structure is a heterophase solid-state morphology. Crazed materials possess unique combinations of mechanical and physical properties including initial linear elasticity, high hysteresis, and recoverability from large strains, an energetically driven retractive force. This behavior is commonly known as "hard elastic," and several investigations have led to hypotheses intended to account for these properties. In crystalline polymers,[12-20] a particular morphology consisting of an aggregate of lamellae layers jointed by profuse small fibrils (crazelike) accounted for this behavior. Some highly crazed amorphous polymers, such as HIPS,[21,22] were discovered in our laboratory to exhibit this unusual phenomenon. Baer and coworkers suggested that the microfibrils in crazed material undergo large elastic deformation and also contribute to a large portion of the elastic recovery.[19-22] It was also found that due to an enormous surface area a large surface energy exists on the microfibrils that contributes a major component of the restoring force in the hard elastic materials.[19-23] A liquid- and vapor-induced stress depression and stress recovery after removal of liquid or vapor has been utilized widely to analyze the contribution of the surface energy and to prove the surprisingly large magnitude of this effect.

The mechanical behavior of flexible PU foams is similar to that of hard elastic materials. In addition, the microcracklike damage that is found on the tension side of deformed struts possesses a morphological structure similar to that in hard elastic materials. The purpose of this study was to apply the liquid-induced stress depression method to probe whether the morphological structure in damaged flexible PU foams exhibited hard elastic behavior. Furthermore, this study explores an analytical methodology[20,21] established for other highly porous hard elastic materials based on this stress depression method. To further confirm the damage processes in cell struts, *in situ* SEM compression experiments were carried out to elucidate the crazing processes occurring in the struts of flexible PU foams during large compressive deformation.

II. EXPERIMENTAL

1. Materials

The materials used in this study were flexible PU foams, generously supplied by the Dow Chemical Company. These foams were made with combinations of Dow's Varanol 3137 polyol and Varanol 3943 copolymer polyol that contain 43% by weight of a finely dispersed SAN copolymer. The average diameter of these SAN particles ranged between 2000 and 3000 Å. The modulus and yield stress increase with increasing SAN copolymer concentrations. Compositions and tensile properties are listed in Table I.

2. Microdeformation in SEM

The morphological structure of strained foam struts were studied by using a specially designed deformation SEM stage that allows deformation in either compression or in tension (Fig. 1). In compression, rectangular block specimens, $5 \times 10 \times 10$ mm^3, were cut from buns and pressed in the direction parallel to the foam rise direction. *In situ* SEM observations in compression on lightly coated (30 Å gold–palladium) samples were carried out up to 75% compressive strain. Dumbbell-shaped tensile specimens with 1 mm thickness, 2 mm width, and 10 mm gauge length were prepared in the direction perpendicular to the foam rise direction. Before being coated with a thin layer (30 Å) of gold–palladium, specimens

Table I Composition and Mechanical Properties of PU Flexible Foams under Compression ($\times 10^{-3}$)

	Foam			
	A	B	C	D
Voranol 3137[a]	100	75	50	0
Voranol 3943[a]	0	25	50	100
Density (g/cm^3)	0.026	0.025	0.025	0.026
Modulus (MPa)[b]	97	190	200	410
Yield stress (MPa)	6.0	8.4	9.8	24

[a] Trademark of the Dow Chemical Company. Voranol 3139: pure polyol; Voranol 3943: SAN copolymer polyol.
[b] Modulus = (load/cross sectional area)/(compression distance/original thickness).

were held at 75% strain in tension. In all instances, the regions of maximum deformation on the strut were examined under a JEOL 840A-CF scanning electron microscope.

3. Cyclic Compression and Stress-Depression Experiments

Rectangular block specimens, 30 × 30 × 50 mm^3, were cut in the direction parallel to the rise direction from foam buns. Cyclic-compression and stress-depression experiments were carried out on an Instron machine with a designed fixture as shown in Figure 2. Foam specimens were compressed at a strain rate of 40% min^{-1} at room temperature.

In the stress-depression measurements, samples were compressed to the desired strain, and then stress was allowed to relax for 1 h to reach a relatively time-independent steady state. The samples were then immersed in an inert, wetting liquid. As soon as the liquid made contact with the sample, the stress dropped rapidly to a new level, which was then allowed to stabilize for 30 min. After the removal of the liquid, the stress recovered completely as the liquid evaporated.

4. Acoustic Emission Monitoring during Compressive Cycling[3]

The acoustic energy dissipation due to the irreversible damage in the foam sample during the cyclic compression in a previous study was monitored by a PAC acoustic emission system made by Physical Acoustic Corporation.

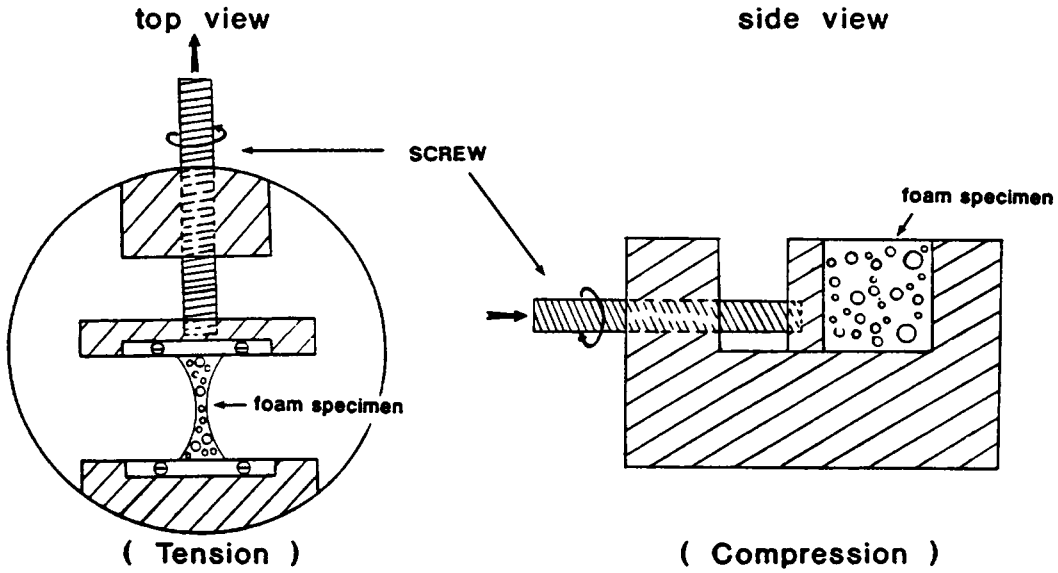

Figure 1 Modified SEM stage for microdeformation experiments.

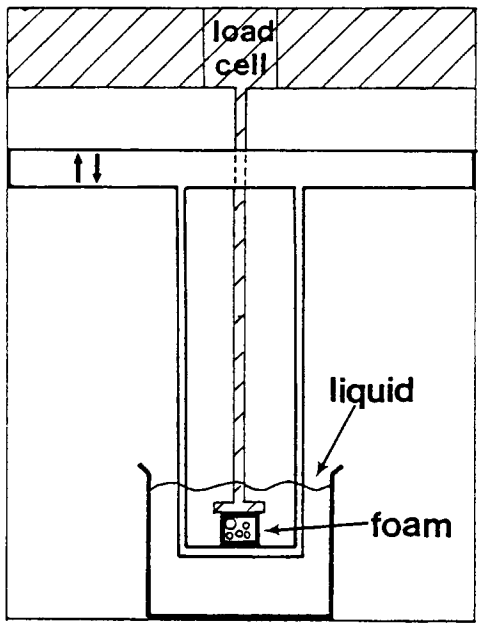

Figure 2 Experimental setup for stress-depression experiment.

III. RESULTS AND DISCUSSION

A. Effects of SAN Concentration on Mechanical Behavior and Damage Processes

1. Mechanical Behavior and Acoustic Emission Dependency on SAN concentration

The cyclic compressive stress–strain behavior of flexible PU foams to 75% strain is shown in Figure 3. Three regions can be differentiated from these curves. In region I, where the foam cell strut joints bend, the material exhibits nominal Hookean behavior. A yield point followed by a plateau is identified as region II, where buckling of struts occurs. In region III, the densification of cell struts gives a sharp increase in the stress. The shapes of these curves in the first two cycles are similar and show a high initial modulus and high recoverability from 75% strain. The larger hysteresis loop of foam D (100% SAN copolymer) when compared to foam C (50% SAN copolymer) indicates that increasing the content of SAN particles leads to an increase in the energy-absorption capability. Similar observations were reported for the energy-absorption capability in foams with different densities[24] and with various loadings of fiber reinforcement.[25] Although these foams have the same density, the higher content of SAN particles gives a higher modulus and yield stress as well as greater energy-absorption capability.

From our previous study,[3] it was found that foam with higher SAN particle concentration leads to more severe damage in the early stage of cyclic fatigue deformation. Figure 4 gives the amount of acoustic emission (which represents the extent of damage) during 1000 cycles fatigue loading on foams C and D. The total number of acoustic emission events in cyclic fatigue of foam D are much larger than that of foam C. This correlates well with the observed greater loss of the mechanical properties of foam D than of foam C in the fatigue test.

2. Progression of Microcracking on the Tension Side of Cell Struts

The effects of the SAN particle concentration on the damage progression was also studied through *in situ* SEM cyclic loading tests.[3] Figure 5 shows the SEM pictures of a buckled strut surface of foam C in the first and 51st cycles. Intense microcracking or crazing occurred on the tension side of a buckled strut in the first cycle and virtually did not change either in craze size or density after 50 cycles. However, in the case of foam D illustrated in Figure 6, the profuse crazing also occurred in the first cycle but became more severe as cycling progressed. Thus, although increasing the amount of SAN particles

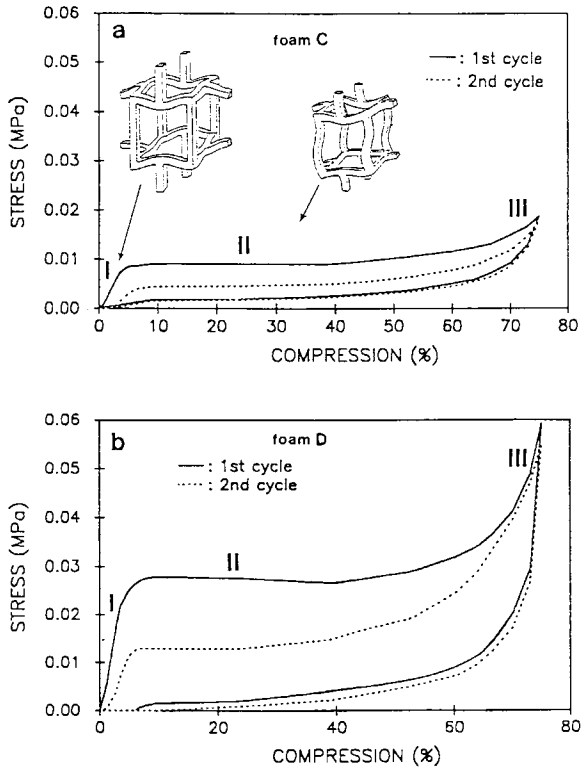

Figure 3 Compressive stress vs. strain curves of foams C and D in cyclic loading.

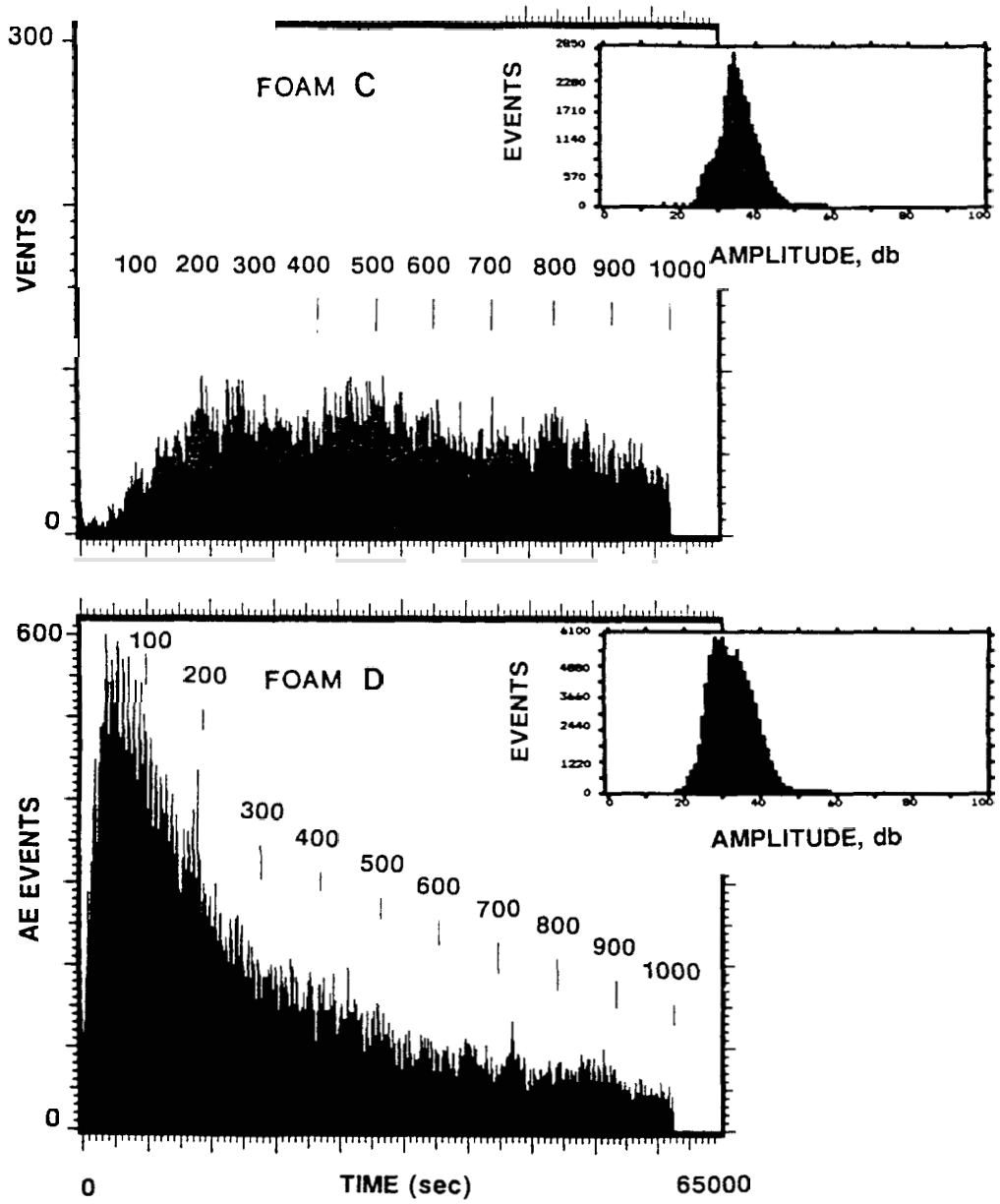

Figure 4 The total number of acoustic emission events in cyclic fatigue of foam D (100% SAN copolymer) and foam C (50% SAN copolymer).[3]

leads to increases in the modulus, buckling stress, and energy-absorption capacity, more severe crazing in the early stages of compressive cyclic loading is observed.

B. Morphological Structure of Cell Struts and Hard Elastic Material

1. In Compression

Since the damage processes in these PU foams are affected by the presence of SAN particles, the morphology of foam D (100% SAN copolymer) was further studied in detail under the scanning electron microscope. Figure 7 illustrates the heterogeneous surface of an undeformed cell strut in foam D with SAN particles visible at 5000×. At 75% compressive strain, this strut buckled with profuse voiding initiating in between SAN particles on the tension side of the strut, as shown in Figure 8. The distance between voids ranged between 0.1 and 0.5 microns. Since the volume fraction of these SAN particles estimated from Figure 7(b) seems to be more than

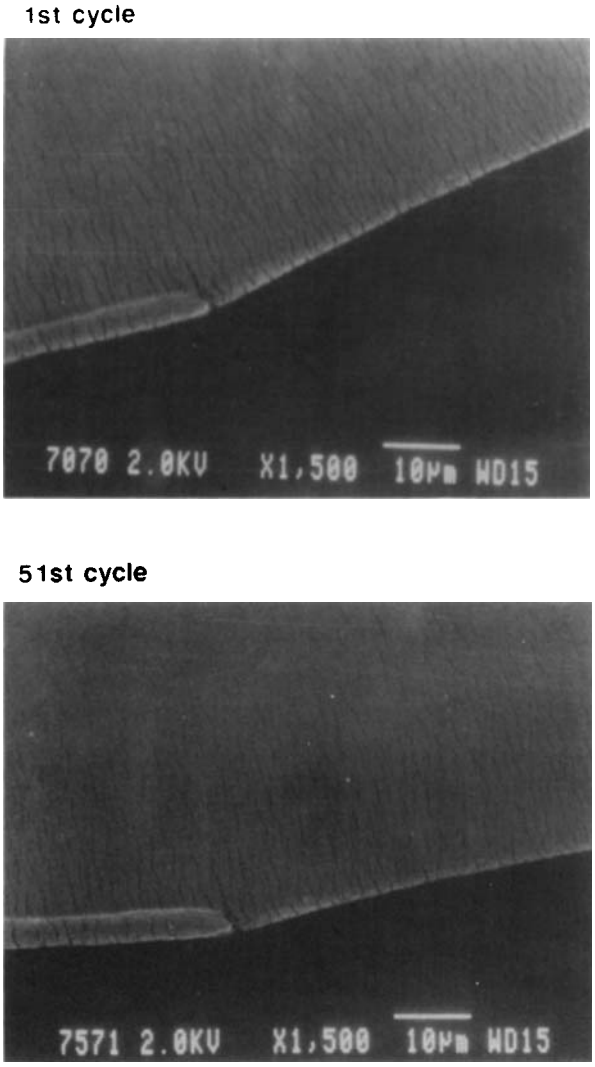

Figure 5 SEM photographs on the surface of a buckled strut in foam C in the first and 51st cycles.[3]

50% and the average diameter of the SAN particles is about 0.3 microns, this suggested that voiding in the cell struts occurred at the boundaries of the SAN particles.

2. *In Tension*

To observe this porous structure more clearly, experiments in tension were carried out in the SEM by stretching foam specimens on a modified SEM stage. Figure 9 shows similar voiding processes as in compression on the surface of a cell strut of foam D at 75% strain. Voiding initiated in between the SAN particles was observed, illustrating again the dilational characteristics of cell struts. Figure 10 shows SEM micrographs of a stretched strut, indicating profuse voids in its 3-dimensional aspect and showing that voiding is not a surface phenomenon. Figure 11(a), which is the higher magnification of Figure 10(a), shows microfibrils within the voids that may contribute to the high recoverability of the foam from large strains. A "large" internal surface area and the overall hierarchical structure of the strained PU foam is reminiscent of the morphological structure of hard elastic material. For comparison, a typical morphological structure of hard elastic material, Celgard 2400, is shown in Figure 11(b), a porous structure with profuse fibrils bridging voids.[21] The microfibrils in crazed material undergo large elastic deformation and contribute to a significant portion of the elastic recovery. Microvoids initiated by the SAN particles promote voiding and the subsequent fibrillation processes. Subsequently, it should be expected that flexible PU foams, with a

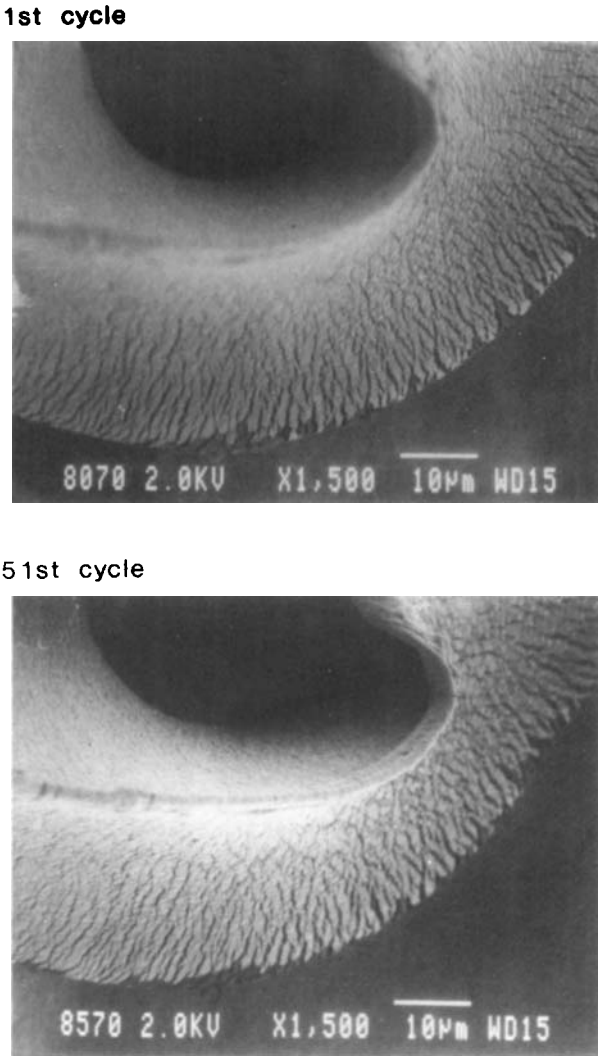

Figure 6 SEM photographs on the surface of a buckled strut in foam D in the first and 51st cycles.[3]

similar morphological structure in the strained state to that of hard elastic materials, may also exhibit the characteristic hard elastic behavior.

C. Factors Affecting the Stress Depression–Hard Elastic Behavior

1. Effects of Surface Tension

Typical stress-depression experiments with foam D were carried in four inert liquids having different values of surface tension. In these experiments, foam samples were compressed to 60% strain and the stress was relaxed for 1 h in order to reach steady state. The samples were then immersed into these liquids, and stress was allowed to stabilize for 30 min and then the liquids were removed. Typical stress depression upon adding liquid is illustrated in Figure 12(a). There was no effect of water, but hexane, isooctane, and hexadecane had significant stress depression. Since these liquids are inert to PU foams, the liquid–polymer interaction is due to surface energy effects. Water, which has high surface tension, could not wet the polymer, and, thus, there was no effect on the stress level. Hexane, isooctane, and hexadecane, on the other hand (due to their relatively low surface tension), caused a spontaneous stress depression upon touching the samples. The stress depression depends on the surrounding medium, confirming that part of the restoring force is due to surface energetics. Previous studies re-

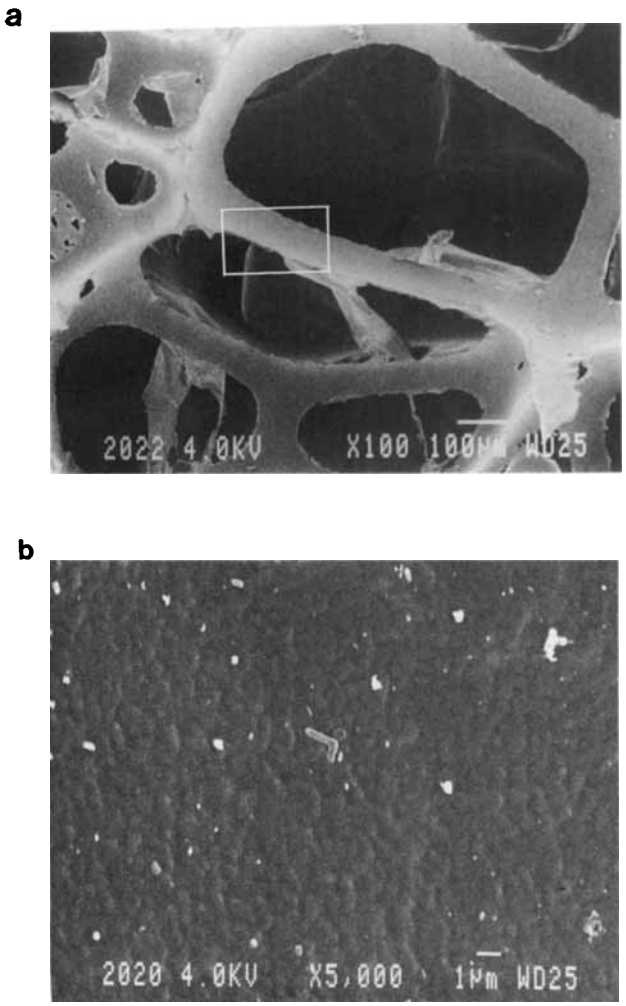

Figure 7 SEM photographs of undeformed foam D in two magnifications: (a) 100×; (b) 5000×.

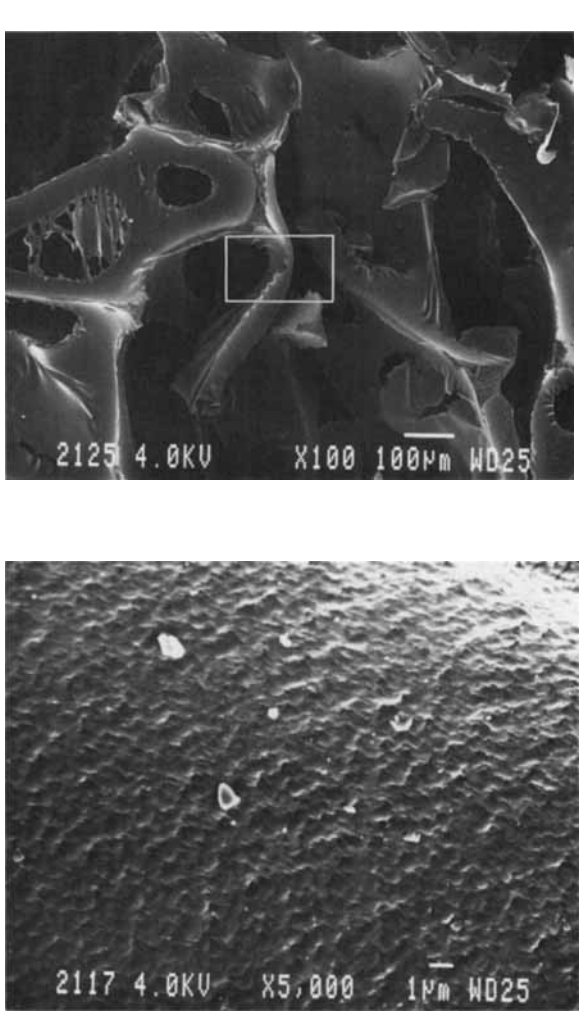

Figure 8 SEM photographs of the same strut as in Figure 7 at 75% compression: (a) 100× shows the buckling struts; (b) 5000× shows voiding initiated in between SAN particles.

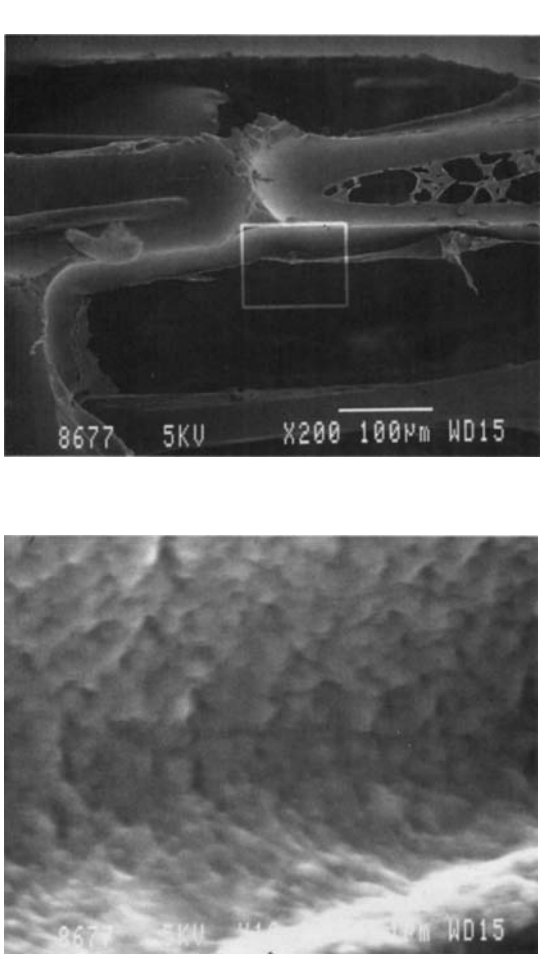

Figure 9 (a) SEM photograph of a strained strut of foam D at 75% in tension. (b) Higher magnification shows the voids in between SAN particles.

ported that microfibrils in a crazed material induce an enormous surface area and that a large surface energy exists on the microfibrils that contributes a significant component of the restoring force in hard elastic materials.[19-23] Figure 12(b) gives an example of the effects of surface tension on the stress depression of hard elastic HIPS.[21]

2. *Effects of Viscosity*

The void characteristics of the strained foam may be determined by the effect of liquid viscosity on the stress depression. Figure 13(a) illustrates the effect of liquid viscosity on the stress drop. In this experiment, silicone oils of different viscosities were used. The shape of the stress curves changes from a rapid stress drop to a more gradual stress reduction as the viscosity is increased from 0.65 to 10 cSt. This phenomenon indicates that the high-viscosity silicone oil may not be able to penetrate the smaller voids inside the struts of the foam in a limited time period of 20 min, which, consequently, reduces the rate of stress depression. The same trends of stress depression in hard elastic HIPS is illustrated in Figure 13(b).[20]

3. *Effects of Compressive Strain*

Since the stress depression is sensitive to the amount of newly created surface area resulting from deformation, the stress depression of PU foams was further investigated as functions of the compressive strain and subsequent changes in the morphological structure. Figure 14(a) illustrates the stress-compression curve of foam D at various compressive

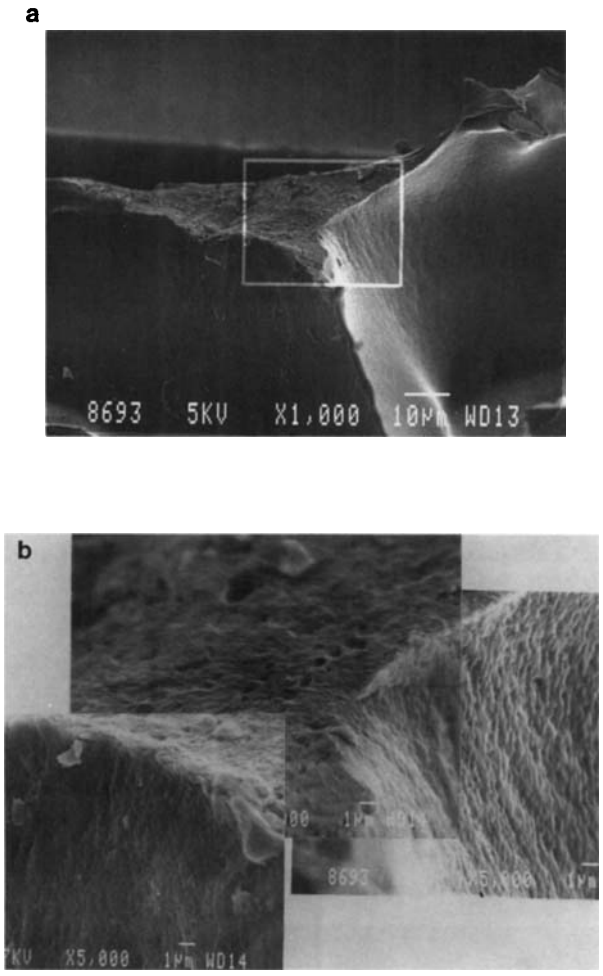

Figure 10 SEM photograph of the surface of a stretched strut showing profuse voiding.

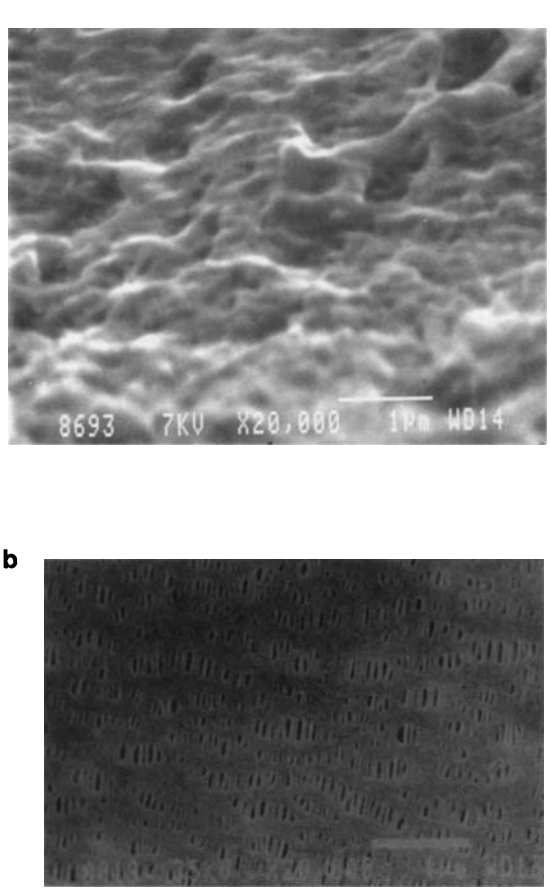

Figure 11 (a) A higher magnification picture of Figure 10 showing voiding with microfibrils. (b) SEM photograph of Celgard 2400—typical morphological structure of a hard elastic material.[21]

strains. It is believed that when the foam sample is compressed in the linear region, new surface is created proportionally to the strain. The amount of stress depression in this region is observed to increase linearly in Figure 14(b). This is further confirmed by the buoyancy nature of the foam in liquid. At 1% compression [Fig. 14(a)], the stress increased rather than dropped upon immersion in hexane and then the stress slightly decreased with time. As the compression increased to 3%, the buoyancy effect diminished and stress depression became dominant upon immersing in liquid. This indicates that at low compression there are few voids and that the stress rise was caused by a buoyancy force.

In the subsequent plateau region, such as at 40% compression where the buckling of struts occurred, the voiding became more profuse. Considerable new surface area was created, resulting in the instant stress depression upon exposure to a wetting liquid. However, at 75 and 95% compressions, the cell struts were totally squeezed together and the whole specimen became densified. Consequently, the penetrating speed of liquid into the cellular structure of the foam specimen was slowed down, resulting only in a gradual stress reduction. However, struts that are subjected to severe deformation at such high strain can open existing voids as well as form new ones. As a result, the amount of stress depression is much larger in this region than in the linear and plateau regions, as illustrated in Figure 15(b). The rate and amount of stress depression at different compressive strains provide the evidence for surface area formation resulting from voiding processes in the strained foam struts.

Based on the changes of morphological structure observed in the previous section, it has been concluded that the presence of SAN particles in foams creates the sites for voiding. Figure 16 illustrates the effects of the amount of SAN particle concentration on the stress depression at 75% compression. A higher content of SAN copolymer causes greater

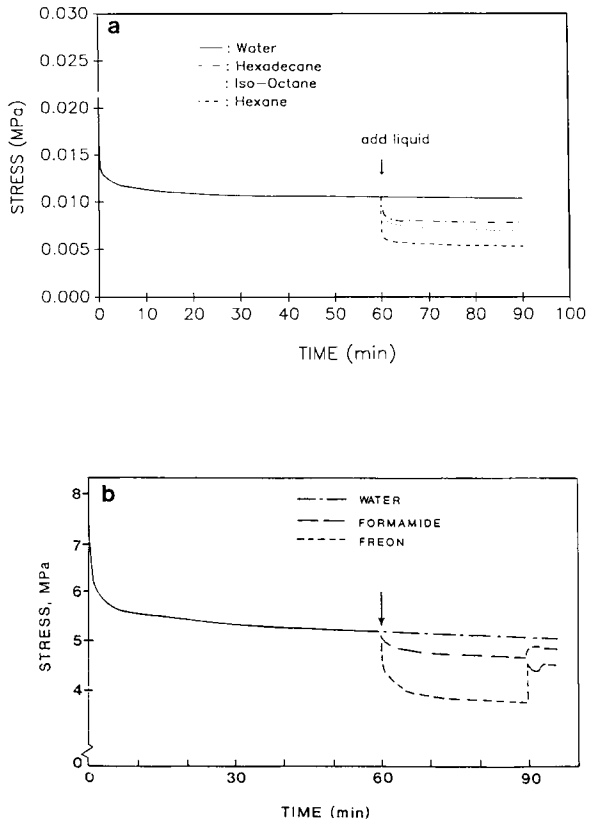

Figure 12 (a) Typical example of stress depression of foam D in various liquids. (b) Stress depression of the hard elastic material (HIPS) in liquids.[21]

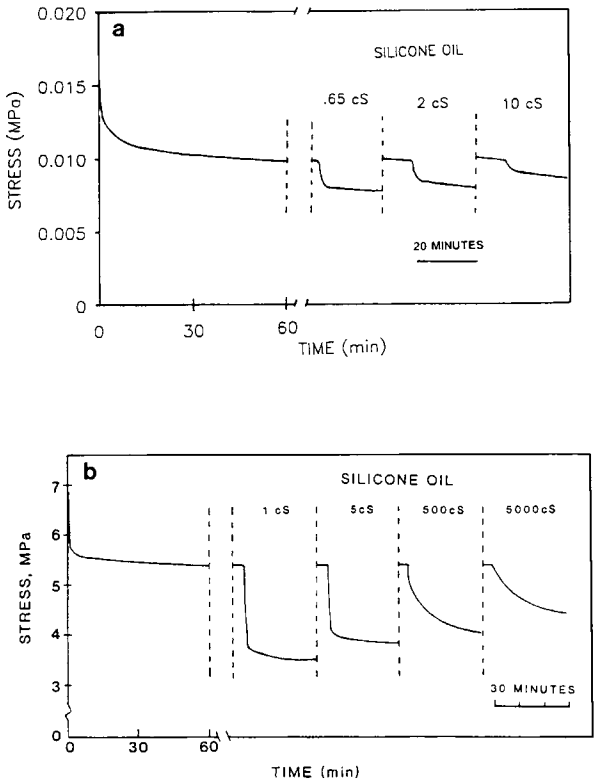

Figure 13 (a) Effects of liquid viscosity on the rate of stress depression. (b) Same phenomenon as observed in hard elastic HIPS.[20]

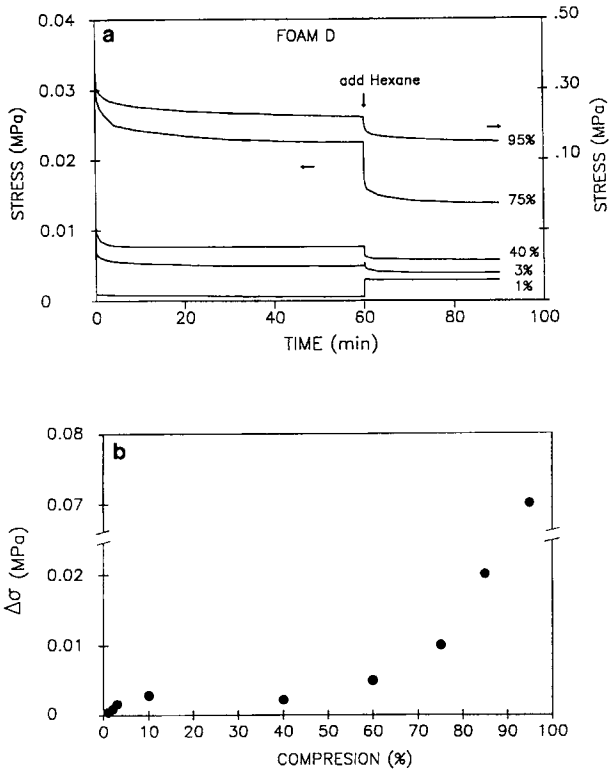

Figure 14 (a) The stress-depression curves of foam D as a function of compression ratio. (b) The amount of stress depression of foam D as a function of compression ratio.

stress depression, confirming that with increasing SAN particles more fresh surface area was created from profuse voiding.

Numerical values of stress depressions at various compressive strains are listed in Table II. The normalized stress depression, which is the ratio of stress depression to the corresponding steady-state stress ($\Delta\sigma/\sigma_t$), shows an almost constant of 35% with no dependence on strain levels. The same phenomenon was reported in hard elastic Celgard[19] and HIPS.[20] A comparison of $\Delta\sigma/\sigma_t$ values of foams to that of hard elastic materials in various liquids, listed in Table III, show that SAN copolymer flexible PU foams have the same characteristic hard elastic behavior.

D. Proposed Model of Voiding Processes

The stress depression in hard elastic materials is associated with newly created surface area of microfibrils inside crazes,[19-23] and surface energy makes a significant contribution to the restoring force. Stress depression is due to the change in surface energy when the wetting liquid is introduced. An analytic method established for Celgard and other porous hard elastic materials,[19,20] which relates stress depression to the microfibrillar structure, is shown below:

$$\Delta\sigma = \frac{4\gamma \cos\theta V_f}{D} \tag{1}$$

where $\Delta\sigma$ = stress depression, γ = surface tension

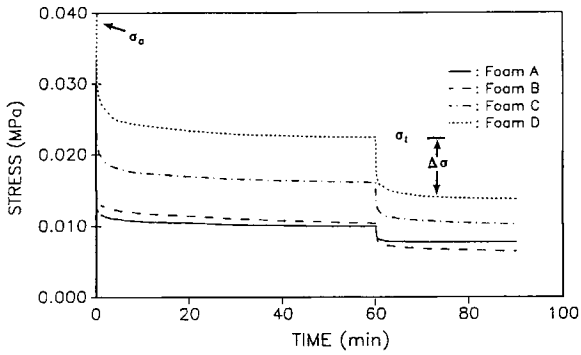

Figure 15 Effect of composition (SAN content) on the stress depression at 75% compression.

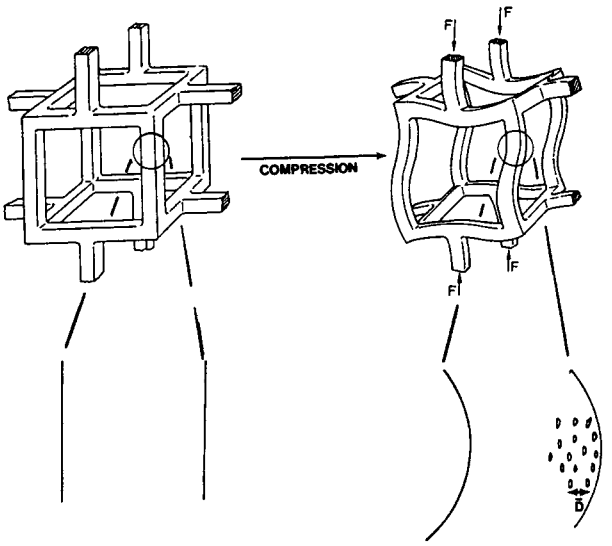

Figure 16 Model of voiding process in a buckled cell strut.

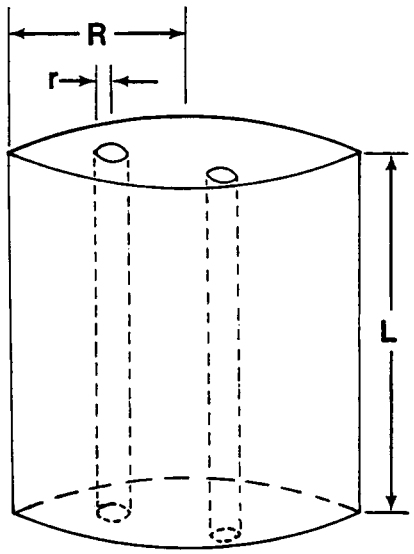

Figure 17 A simplified model assuming foam as a cylinder composed by struts, (subcylinder) in the cellular structure.

of the liquid, θ = contact angle, V_f = volume fraction of the fibril, and D = average fibril diameter.

Voiding in the struts has been identified as the dominated surface process, suggesting that the strained struts are composed of numerous crazes containing many subfibrils that are separated by voids. A simplified model of the cell strut voiding process is proposed in Figure 16. The volume fraction of fibril (V_f) in the case of strained foam becomes the volume fraction of material in the voided struts and equals one. Hence,

$$\Delta\sigma_{\text{actual}} = \frac{4\gamma \cos\theta}{D} \tag{2}$$

$$\Delta\sigma_{\text{apparent}} = \Delta\sigma_{\text{actual}} \times A_f \tag{3}$$

where $\Delta\sigma_{\text{apparent}}$ is the observed stress depression based on the total cross-sectional area of the foam sample and the actual stress depression ($\Delta\sigma_{\text{actual}}$) results from the change of surface energy on the struts. Therefore, the cross-sectional area fraction of struts in foam sample (A_f) is used for this correction. A_f can be obtained by assuming the foam sample as a cylinder composed of subcylinders that represents struts in the foam sample, as illustrated in Figure 17. It follows that

$$A_f = \frac{\pi r^2}{\pi R^2} = \frac{\pi r^2 L}{\pi R^2 L} = V_{f0} = \frac{\rho_f}{\rho_s} \tag{4}$$

where V_{f0} = volume fraction of struts in foam, ρ_f = density of foam sample, and ρ_s = density of solid PU.

Table II Stress Depressions of PU Foams in Hexane as a Function of Compressive Strain (MPa $\times 10^{-3}$)

Compression (%)	Foam A				Foam B				Foam C				Foam D			
	σ_0	σ_t	$\Delta\sigma$	$\Delta\sigma/\sigma_t$	σ_0	σ_t	$\Delta\sigma$	$\Delta\sigma/\sigma_t$	σ_0	σ_t	$\Delta\sigma$	$\Delta\sigma/\sigma_t$	σ_0	σ_t	$\Delta\sigma$	$\Delta\sigma/\sigma_t$
1									1.1	1.0	0.22	22	1.0	0.6	0.41	68
2									1.8	1.6	0.44	28	3.9	2.3	0.88	38
3									4.3	2.9	0.73	25	7.8	4.8	1.6	33
10	5.1	3.1	0.83	27	5.8	2.8	1.2	44	8.3	4.5	1.3	29	13	6.3	2.9	46
40	6.0	3.9	1.1	27	6.5	3.7	1.4	37	7.7	4.7	1.1	23	13	5.8	2.2	38
60	6.2	4.4	1.0	23	9.4	5.7	2.1	37	12	7.2	1.8	25	22	12	5.0	42
75	15	10	2.5	25	17	11	4.2	38	29	17	5.8	34	45	26	10	39
85													112	53	20	38
95													455	221	70	32

Table III Stress Depression of Various Hard Elastic Materials in Liquid

Polymer/Liquid	σ_t (MPa)	$\Delta\sigma$ (MPa)	$\Delta\sigma/\sigma_t$ (%)
Celgard 2400/ethanol[19]	30.5	13.7	45
HIPS/freon[21]	5.2	1.4	25
HEPP/ethanol[20]	—	—	46

By substituting A_f in (4) into (3),

$$\sigma_{\text{actual}} = \frac{\sigma_{\text{apparent}}}{(\rho_f/\rho_s)} \tag{5}$$

Equation (2) is then rearranged by substituting σ_{actual} in (5) and

$$D = \frac{4\gamma \cos\theta}{\Delta\sigma_{\text{apparent}}/(\rho_f/\rho_s)} \tag{6}$$

Equation (6) can be applied to estimate the average distance between voids in strained cell struts. Table IV lists the average distance (D) in between voids. In the linear region, D decreases gradually and levels off in plateau regions, and in the densification region, the value decreases again. It is believed that voids are generated gradually in the linear region with increasing compression, causing the decrease of the D value. While in the plateau region, the constant value of D suggests that coalescence of voids may occur when struts buckle and that the distance between voids remains essentially constant. In the densification region, decrease of the D value again suggests that more voids were generated.

At 60 and 75% compression, the calculated D values were 0.32 and 0.16 microns. From SEM observations, D values between 0.1 and 0.5 microns were observed. The average diameter of SAN particles was about 0.3 microns, indicating that voiding probably initiated at the boundaries of SAN particles. Foam D, which has the highest amount of SAN copolymer, had the lowest D values. Foam D also had more voids than did the other foams, indicating that the presence of SAN particles provides stress-concentration sites, resulting in more profuse voiding that gives rise to larger stress depression.

CONCLUSIONS

The phenomena of profuse voiding in strained cell struts and the observed stress depression when this hierarchical foam structure is exposed to wetting by inert liquids have been utilized to prove that this type of flexible PU foams has a similar morphological structure in the strained state as that of hard elastic materials. The presence of SAN particles that increase the modulus and the plateau stress also are the sites for localized stress concentrations. When strained, the foam struts became highly porous when voiding initiates in between the SAN particles. This voiding was confirmed by direct scanning electron microscopy and a mechanistic model based on the stress-depression method. This method, which was previously established for other highly porous hard elastic materials, was modified to obtain the distance between voids, and the calculated values of around 0.3 microns were in good agreement with observations from scanning electron micrographs.

Table IV Stress Depression and the Calculated Distance in between Voids as a Function of Compression Ratio

Compression (%)	Foam A		Foam B		Foam C		Foam D	
	$\Delta\sigma$ ($\times 10^{-3}$ MPa)	D (μm)	$\Delta\sigma$	D	$\Delta\sigma$	D	$\Delta\sigma$	D
1					0.22	7.1	0.41	3.9
2					0.44	3.5	0.88	1.8
3					0.73	2.1	1.6	1.0
10	0.83	2.0	1.2	1.3	1.3	1.2	2.9	0.56
40	1.1	1.5	1.4	1.1	1.1	1.4	2.2	0.74
60	1.0	1.6	2.1	0.74	1.8	0.86	5.0	0.32
75	2.5	0.65	4.2	0.37	5.8	0.27	10	0.16
85							20	0.08
95							70	0.02

The authors wish to thank the Dow Chemical Company, Freeport, Texas, for their financial support of this work.

REFERENCES

1. E. T. Lloyd and G. M. Gray, *J. Cell. Plast.*, **15,** 47 (1979).
2. L. F. Lawlyer, Y. Televantos, G. Combs, and S. N. Gablnem, *J. Cell. Plast.*, **25,** 231 (1989).
3. C. Kau, L. Huber, A. Hiltner, and E. Baer, to appear.
4. C. G. Seefried, Jr., R. D. Whitman, and D. F. Pollart, *J. Cell. Plast.*, **10,** 17 (1974).
5. B. Beals, F. J. Dwyer, and M. Kaplan, *J. Cell. Plast.*, **1,** 32 (1965).
6. F. J. Dwyer, *J. Cell. Plast.*, **12,** 104 (1976).
7. R. P. Kane, *J. Cell. Plast.*, **1,** 217 (1965).
8. R. B. Turner and G. L. Wilkes, in *Structure vs. Properties of Flexible Urethane Foams Used in the Home Furnishing Industry (Polymer-Morphology),* Kurt Frisch Symposium, University of Detroit, Detroit, IL, January 1988.
9. W. M. Lee, *J. Cell. Plast.*, **20,** 369 (1984).
10. R. Caspary and H. W. Schnecko, *Makromol. Chem.*, **182,** 2109 (1981).
11. Q. Zhao, R. E. Marchant, J. M. Anderson, and A. Hiltner, *Polymer,* **28,** 2041 (1987).
12. S. L. Cannon, W. O. Statton, and J. W. S. Hearle, *Polym. Eng. Sci.*, **15**(19), 633 (1975).
13. M. Miles, J. Petermann, and H. Gleiter, *J. Macromol. Sci. Phys.*, **B12**(4), 523 (1976).
14. T. Hashimoto, A. Tsukahara, and H. Kawai, *Polymer,* **20,** 636 (1979).
15. I. K. Park and H. D. Noether, *Colloid Polym. Sci.*, **253,** 824 (1975).
16. T. Yamazaki, S. Oys, N. Tsukane, H. Toba, and K. Yamagishi, *Polymer,* **16,** 425 (1975).
17. B. S. Sprague, *J. Macromol. Sci. Phys.*, **B8**(1–2), 157 (1973).
18. T. Tanigami, K. Yamaura, S. Matsuzawa, K. Ohsawa, and K. Miyasaka, *J. Appl. Polym. Sci.*, **32,** 4491 (1986).
19. C. J. Chou, A. Hiltner, and E. Baer, *Polymer,* **27,** 369 (1986).
20. K. Walton, A. Moet, and E. Baer, *Contemporary Topics in Polymer Science,* Vol. 4, Plenum, New York, 1982.
21. A. Moet, L. Palley, and E. Baer, *J. Appl. Phys.*, **51**(10), 5175 (1980).
22. M. J. Miles and E. Baer, *J. Mater. Sci.*, **14,** 1254 (1979).
23. H. Brown and E. Kramer, *Polymer,* **22,** 689 (1981).
24. P. E. Kreter, *J. Cell. Plast.*, **21,** 306 (1985).
25. Z. Korzeniowski and K. Piekarski, *J. Cell. Plast.*, **11,** 37 (1975).

Received June 4, 1991
Accepted June 25, 1991